Effective *s*- and *p*-wave contact interactions in trapped degenerate Fermi gases

R. Roth* and H. Feldmeier†
Gesellschaft für Schwerionenforschung (GSI), Planckstrasse 1, 64291 Darmstadt, Germany
(Received 22 February 2001; published 12 September 2001)

The structure and stability of dilute degenerate Fermi gases trapped in an external potential is discussed with special emphasis on the influence of *s*- and *p*-wave interactions. In a first step an effective contact interaction for all partial waves is derived, which reproduces the energy spectrum of the full potential within a mean-field model space. Using the *s*- and *p*-wave part the energy density of the multicomponent Fermi gas is calculated in Thomas-Fermi approximation. On this basis the stability of the one- and two-component Fermi gas against mean-field induced collapse is investigated. Explicit stability conditions in terms of density and total particle number are given. For the single-component system attractive *p*-wave interactions limit the density of the gas. In the two-component case a subtle competition of *s*- and *p*-wave interactions occurs and gives rise to a rich variety of phenomena. A repulsive *p*-wave part, for example, can stabilize a two-component system that would otherwise collapse due to an attractive *s*-wave interaction. It is concluded that the *p*-wave interaction may have important influence on the structure of degenerate Fermi gases and should not be discarded from the outset.

DOI: 10.1103/PhysRevA.64.043603 PACS number(s): 03.75.Fi, 32.80.Pj, 34.20.Cf

I. INTRODUCTION

The achievement of Bose-Einstein condensation in trapped dilute gases of bosonic atoms [1] triggered a widespread interest in the field of ultracold atomic gases. Meanwhile these systems appear as a unique laboratory for the study of all kinds of fundamental quantum phenomena.

After a series of excellent experiments on bosonic systems, the question arises whether a dilute gas of fermionic atoms can also be cooled to temperatures where quantum effects dominate. In 1999 DeMarco and Jin managed to cool a sample of typically 10^6 fermionic ^{40}K atoms to temperatures significantly below the Fermi energy of the system [2]; in recent experiments they achieved a temperature corresponding to one-fifth of the Fermi energy [3]. By sympathetic cooling of fermionic ^{6}Li with bosonic ^{7}Li Truscott *et al*. were able to reach about one-fourth of the Fermi energy [4]. In these temperature regimes the system can be described as a degenerate Fermi gas, where the majority of the atoms successively fills the lowest available one-body states according to the Pauli principle.

One of the goals of the investigations on dilute and ultracold Fermi gases is the observation of Cooper pairing and the transition to a superfluid state. The transition temperature depends on the density and on the strength of the attractive interaction that is necessary for the formation of Cooper pairs [5,6]. In order to increase the transition temperature one may increase the density or the interaction strength, where the latter seems to be more promising. An atomic species favored for the experimental observation of a BCS transition is ^{6}Li due to its large *s*-wave scattering length of $a_0 \approx -2160 a_B$ [7]. But also ^{40}K, which shows a rather small natural scattering length, is a possible candidate for Cooper pair formation [3], because a simultaneous *s*- and *p*-wave Feshbach resonance is predicted [8], which allows tuning of the *s*- and *p*-wave scattering lengths over a very wide range.

A serious constraint on the way towards a superfluid Fermi gas is the mechanical stability of the progenitor, i.e., the normal degenerate Fermi gas. As was experimentally demonstrated for the bosonic ^{85}Rb system [9], an attractive interaction between the atoms leads to a mean-field instability of the trapped gas if the density exceeds a critical value. A similar collapse is expected in fermionic systems with attractive interactions. In contrast to the bosonic systems *p*-wave interactions contribute in a Fermi gas and may have strong influence on the stability of the system [10].

In the following we address the question of the stability of degenerate one- and two-component Fermi gases in the presence of *s*- and *p*-wave interactions within a simple and transparent model. In Sec. II we derive an effective contact interaction (ECI) for all partial waves that is suited for a mean-field treatment of the many-body problem. Using the *s*- and *p*-wave part of this interaction we construct in Sec. III the energy functional of a trapped multicomponent Fermi gas in the Thomas-Fermi approximation. From that the ground-state density profile can be determined by functional variation. In Sec. IV we discuss the structure and stability of single-component Fermi gases, where only the *p*-wave interaction contributes according to the Pauli principle. Section V deals with two-component Fermi gases where *s*- and *p*-wave interactions are present and lead to a subtle dependence of the stability on the two scattering lengths.

II. EFFECTIVE CONTACT INTERACTION

A. Concept

The approximate solution of the many-body problem in a restricted subspace of the full Hilbert space, which is spanned by plane waves with momenta smaller than the Fermi momentum, faces a fundamental problem: Many realistic two-body interactions—like van der Waals–type interactions between atoms or the interactions between two nucleons in an atomic nucleus—exhibit a strong repulsion at

*Electronic address: r.roth@gsi.de;
URL: http://theory.gsi.de/~trap/
†Electronic address: h.feldmeier@gsi.de

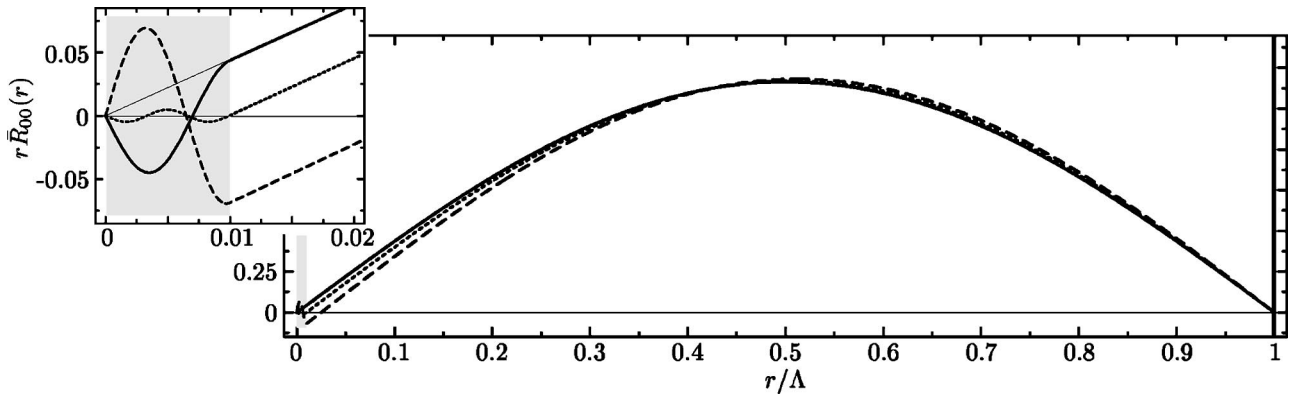

FIG. 1. Radial wave functions $r\overline{R}_{00}(r)$ of the lowest $l=0$ positive-energy state for different potential depths V_0 of the square-well potential. The interaction strengths are $\lambda\sqrt{V_0}=0$ (thin solid), 4.49 (solid), 4.85 (dashed), and 9.5 (dotted). The radius of the well is $\lambda=0.01\Lambda$ and marked by the gray area. The inset shows a magnification of the region around the origin.

short distances followed by an attractive region. This causes the wave function of a low-energy scattering state to vary rapidly within the range of the potential (see Fig. 1). These high-momentum components, however, cannot be described within the low-momentum model space [11]. Therefore a realistic two-body interaction cannot be used in a naive mean-field model. One way to overcome this problem in the model space is to introduce a suitable effective interaction that has to be deduced from the original potential and depends on the properties of the actual physical system under investigation.

Cold and very dilute quantum gases allow an effective interaction of simple structure. The typical wavelength of the relative motion of two particles is always large compared to the range of the interaction. Therefore the particles experience only an ''averaged'' two-body potential and do not probe the detailed radial dependence. Moreover, the gases are in a metastable not-self-bound state that is kept together by the external trapping potential. Thus the bound states of the two-body potential are not populated and have only indirect influence. We make use of these facts and replace the original potential by a contact interaction. The strengths of the contact terms are related to the properties of the original potential.

We establish this relation via the energy spectrum of the two-body system. Consider a two-body problem with an auxiliary boundary condition at some large radius such that the spectrum is discrete even for positive energies. For noninteracting particles this spectrum shows a sequence of levels at positive energies E_{nl}, which are labeled by an angular momentum quantum number l and a radial quantum number n. A schematic sketch of this spectrum for some fixed l is shown in Fig. 2. If we switch on an interaction between the particles two things happen: A number n_l^b of bound two-body states with relative angular momentum l may appear at negative energies and the levels at positive energies $\overline{E}_{nl}$ are shifted compared to the noninteracting spectrum. For our purpose this energy shift $\Delta E_{nl}=\overline{E}_{nl}-E_{nl}$ is defined between the positive-energy states only. The lowest level of positive energy is labeled with the quantum number $n=0$.

Since we want to construct an effective Hamiltonian that is used to calculate the energy in a mean-field framework, the energy shift is the relevant property of the two-body potential that the effective interaction should reproduce. We require that the expectation values of the effective interaction calculated with eigenstates $|nlm\rangle$ of the noninteracting two-body system equal the energy shifts ΔE_{nl} induced by the original potential

$$\langle nlm|v^{\mathrm{eff}}|nlm\rangle=\overline{E}_{nl}-E_{nl}=\Delta E_{nl}. \tag{1}$$

Due to the angular momentum dependence of the energy shifts we have to construct the effective contact interaction as a sum of contact terms for each partial wave. The strength of each contact term is fixed by this condition.

B. Construction of the ECI

The construction of the effective contact interaction (ECI) is organized in two steps: Firstly, the two-body energy shift induced by the original potential is evaluated. Secondly, the

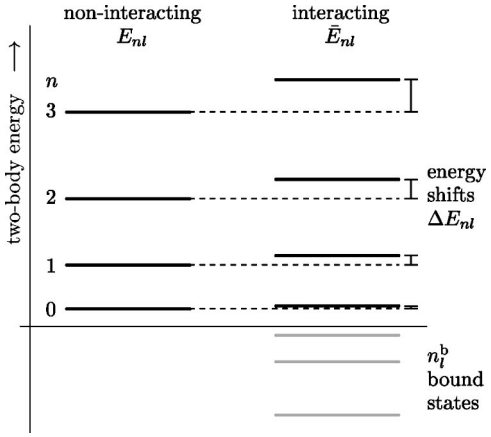

FIG. 2. Schematic comparison of the free two-body energy spectrum E_{nl} with the energy spectrum $\overline{E}_{nl}$ in the presence of a two-body interaction for given relative angular momentum l. The interaction generates n_l^b bound states and shifts the positive-energy states by ΔE_{nl}.

operator of the effective contact interaction is formulated for each partial wave and the interaction strengths are fixed by condition (1).

1. Energy shift

Assume a system of two particles with reduced mass $m_{\rm red}=m_1m_2/(m_1+m_2)$. Their wave function can be decomposed into a center of mass and a relative wave function, where the latter separates into a radial and an angular component because of rotational symmetry

$$\langle\vec{r}|nlm\rangle=R_{nl}(r)Y_{lm}(\Omega). \tag{2}$$

The radial wave functions $R_{nl}(r)$ of the noninteracting two-body system are solutions of the Schrödinger equation

$$\left[-\frac{1}{r}\frac{\partial^2}{\partial r^2}r+\frac{l(l+1)}{r^2}-2m_{\rm red}E_{nl}\right]R_{nl}(r)=0 \tag{3}$$

(we use units with $\hbar=1$). We require the radial wave function to vanish at some arbitrary but large radius Λ

$$R_{nl}(\Lambda)=0. \tag{4}$$

This auxiliary boundary condition leads to a discrete energy spectrum, which is needed to enumerate the energy levels and to evaluate the energy shift.

In the noninteracting case the solution of the radial Schrödinger equation (3) is given by a spherical Bessel function $j_l(x)$

$$R_{nl}(r)=A_{nl}j_l(q_{nl}r), \tag{5}$$

where q_{nl} denotes the relative momentum of the two particles and A_{nl} a normalization constant. The discrete momenta q_{nl} are determined by the boundary condition (4) and thus are related to the zeros of the Bessel function. Since the radius Λ can be chosen arbitrary large it is sufficient to use the asymptotic expansions of the spherical Bessel and Neumann functions

$$j_l(x)=\frac{1}{x}\sin(x-\pi l/2),\quad x\gg l,$$

$$n_l(x)=-\frac{1}{x}\cos(x-\pi l/2),\quad x\gg l. \tag{6}$$

By evaluating the boundary condition (4) with the asymptotic form of the Bessel function we obtain for the possible relative momenta

$$q_{nl}\Lambda=\pi(n+l/2). \tag{7}$$

Accordingly the two-body energy spectrum in the noninteracting case is given by

$$E_{nl}=\frac{1}{2m_{\rm red}}q_{nl}^2=\frac{\pi^2}{2m_{\rm red}\Lambda^2}(n+l/2)^2. \tag{8}$$

The normalization constant can be determined explicitly

$$A_{nl}^{-2}=\int_0^\Lambda dr\,r^2j_l^2(q_{nl}r)=\frac{\Lambda^3}{2}j_{l+1}^2(q_{nl}\Lambda). \tag{9}$$

Inserting the asymptotic form of the Bessel function we finally get

$$A_{nl}^{-2}=\frac{\Lambda}{2q_{nl}^2},\quad q_{nl}\Lambda\gg l. \tag{10}$$

In the presence of a two-body potential $v(r)$ of finite range λ the solution $\overline{R}_{nl}(r)$ of the Schrödinger equation

$$\left[-\frac{1}{r}\frac{\partial^2}{\partial r^2}r+\frac{l(l+1)}{r^2}+2m_{\rm red}[v(r)-\overline{E}_{nl}]\right]\overline{R}_{nl}(r)=0 \tag{11}$$

outside the range of the potential ($r>\lambda$) is given by a superposition of spherical Bessel and Neumann functions

$$\overline{R}_{nl}(r)=\overline{A}_{nl}[j_l(\overline{q}_{nl}r)-\tan\eta_l(\overline{q}_{nl})n_l(\overline{q}_{nl}r)], \tag{12}$$

where $\eta_l(q)$ denotes the phase shift of the potential for the lth partial wave. The bar distinguishes quantities in the presence of the interaction from those in the noninteracting case. Imposing the boundary condition (4) we get the following implicit equation for the momenta $\overline{q}_{nl}$ in the interacting case:

$$\frac{j_l(\overline{q}_{nl}\Lambda)}{n_l(\overline{q}_{nl}\Lambda)}=\tan\eta_l(\overline{q}_{nl}). \tag{13}$$

Expressing the Bessel and Neumann functions by their asymptotic expansion (6) this reduces to

$$-\tan(\overline{q}_{nl}\Lambda-\pi l/2)=\tan\eta_l(\overline{q}_{nl}). \tag{14}$$

In order to associate the energy levels with the same quantum number n in the interacting and noninteracting case as described above, the lowest positive-energy state should be labeled with the quantum number $n=0$. To achieve this for a potential with n_l^b bound two-body states with angular momentum quantum number l we add the phase $\pi(n+n_l^b)$ to the argument on the right-hand side (rhs), i.e., the bound states contribute according to Levinson's theorem. The momenta $\overline{q}_{nl}$ in the presence of the interaction are thus determined by the equation

$$\overline{q}_{nl}\Lambda=-\eta_l(\overline{q}_{nl})+\pi(n+n_l^b+l/2). \tag{15}$$

The momentum shift Δq_{nl} induced by the interaction is obtained by subtracting the momenta of the noninteracting system (7) from Eq. (15)

$$\Delta q_{nl}\Lambda=(\overline{q}_{nl}-q_{nl})\Lambda=-[\eta_l(\overline{q}_{nl})-\pi n_l^b]=-\tilde{\eta}_l(\overline{q}_{nl}). \tag{16}$$

Here $\tilde{\eta}_l(q)=\eta_l(q)-\pi n_l^b$ denotes the phase shift reduced by the contribution of the bound states. In a final step we expand the phase shifts around the momenta q_{nl} of the noninteracting system

$$\tilde{\eta}_l(\overline{q}_{nl}) = \tilde{\eta}_l(q_{nl}) + \tilde{\eta}_l'(q_{nl})\Delta q_{nl} + \cdots . \tag{17}$$

Already the term linear in Δq_{nl} can be neglected in good approximation because the momentum shift is of the order $1/\Lambda$ according to Eq. (16). Thus we retain the following simple expression for the momentum shift:

$$\Delta q_{nl}\Lambda = -\tilde{\eta}_l(q_{nl}). \tag{18}$$

The shift of the energy levels of the interacting two-body system compared to the noninteracting spectrum is connected with the momentum shift by

$$\frac{\Delta E_{nl}}{E_{nl}} = 2\frac{\Delta q_{nl}}{q_{nl}} + \left(\frac{\Delta q_{nl}}{q_{nl}}\right)^2. \tag{19}$$

The term quadratic in the momentum shift can be neglected because $\Delta q_{nl}/q_{nl}$ is small. The final expression for the energy shift reads

$$\frac{\Delta E_{nl}}{E_{nl}} = -\frac{2}{\Lambda}\frac{\tilde{\eta}_l(q_{nl})}{q_{nl}}. \tag{20}$$

The proportionality between energy shift and phase shifts is well known [12] and was used in different applications before.

2. ECI in scattering length approximation

In a second step we construct an operator form of the effective contact interaction that obeys condition (1). For the application to ultracold dilute quantum gases the general form (20) of the energy shift ΔE_{nl} can be simplified considerably. The relative momenta in these systems are extremely low, i.e., typical relative wavelengths are large compared to the range of the interaction. This allows an expansion of the phase shifts $\tilde{\eta}_l(q)$ in a power series in relative momentum. In lowest-order approximation ($qa_l \ll 1$) the phase shifts of the lth partial wave can be expressed in terms of the corresponding scattering length a_l[1],

$$\frac{\tilde{\eta}_l(q)}{q^{2l+1}} \approx \frac{\tan\eta_l(q)}{q^{2l+1}} \approx -\frac{(2l+1)}{[(2l+1)!!]^2}a_l^{2l+1}, \tag{21}$$

The energy shift in this scattering length approximation is given by

$$\frac{\Delta E_{nl}}{E_{nl}} = \frac{2}{\Lambda}\frac{(2l+1)}{[(2l+1)!!]^2}q_{nl}^{2l}\,a_l^{2l+1}. \tag{22}$$

Based on this form we can construct a simple operator for the ECI. For applications where approximation (21) is not sufficient higher-order terms of the power series can be included successively. We will come back to this point in the following section.

According to the dependence of the energy shifts on the angular momentum quantum number l the operator of the effective interaction $v^{\rm eff}$ is formulated as a sum of independent operators $v_l^{\rm eff}$ for each partial wave

$$v^{\rm eff} = \sum_{l=0}^{\infty} \Pi_l\, v_l^{\rm eff}\, \Pi_l, \tag{23}$$

where Π_l denotes the projection operator on the subspace spanned by states of relative angular momentum l. We want to use a contact interaction for each partial wave. This requires nonlocal interaction operators beyond $l=0$, i.e., derivative couplings. The simplest ansatz for the operator of the effective contact interaction for the lth partial wave is

$$\begin{aligned} v_l^{\rm eff} &= (\vec{q}\cdot\hat{r})^l g_l\ \delta^{(3)}(\vec{r})\ (\hat{r}\cdot\vec{q})^l \\ &= \int d^3r\ |\vec{r}\rangle \frac{\overleftarrow{\partial}^l}{\partial r^l} g_l\ \delta^{(3)}(\vec{r})\ \frac{\overrightarrow{\partial}^l}{\partial r^l}\langle\vec{r}|. \end{aligned} \tag{24}$$

Here $\vec{q} = \frac{1}{2}(\vec{p}_1 - \vec{p}_2)$ denotes the operator of the relative momentum of two particles, $\hat{r} = \vec{r}/r$ denotes the unit vector along the relative coordinate, and $\delta^{(3)}(\vec{r}) = 1/(4\pi r^2)\delta(r)$ denotes the radial component of the three-dimensional δ function. The arrows above the derivatives indicate to which side they act.

Notice that this type of effective interaction is constructed to be used within the restricted low-momentum model space only. It does not make sense to employ it for the solution of the full Schrödinger equation or for a perturbative treatment beyond lowest order.

The interaction strength g_l is a constant that contains the relevant information on the original two-body potential. The connection is provided by condition (1) via the shift of the energy levels with respect to the free spectrum. To evaluate (1) we calculate the expectation value of the contact interaction (24) for the lth partial wave taken with the noninteracting two-body states $|nlm\rangle$,

$$\begin{aligned} \langle nlm|v_l^{\rm eff}|nlm\rangle &= g_l \int d^3r\, \delta^{(3)}(\vec{r}) \left|\frac{\partial^l}{\partial r^l} R_{nl}(r) Y_{lm}(\Omega)\right|^2 \\ &= \frac{g_l}{4\pi}\left|\frac{\partial^l}{\partial r^l} R_{nl}(r)\right|^2_{r=0} \\ &= \frac{g_l}{4\pi}\left[\frac{l!}{(2l+1)!!}\right]^2 A_{nl}^2\, q_{nl}^{2l}, \end{aligned} \tag{25}$$

where we used the expansion of the radial wave function around the origin

$$R_{nl}(r) = A_{nl}\frac{(q_{nl}r)^l}{(2l+1)!!}\left[1 - \frac{(q_{nl}r)^2}{2(2l+3)} + \cdots\right]. \tag{26}$$

[1]Some authors [8] use a different definition of the p-wave scattering length without the l-dependent prefactors. We use this general form (see [16]) where the scattering length for a hard sphere equals the sphere radius for all l.

Equating the expectation value (25) with the energy shift results in the following equation for the interaction strengths:

$$g_l = 4\pi \left[\frac{(2l+1)!!}{l!} \right]^2 A_{nl}^{-2} \frac{\Delta E_{nl}}{q_{nl}^{2l}}. \tag{27}$$

Inserting the normalization constant (10) and the energy shift in scattering length formulation (22) gives the final expression for the interaction strengths

$$g_l = \frac{4\pi}{2m_{\mathrm{red}}} \frac{(2l+1)}{(l!)^2} a_l^{2l+1}. \tag{28}$$

Together with Eq. (24) this defines the scattering length formulation of the effective contact interaction. Notice that these expressions do not depend on the auxiliary boundary condition (4), which was introduced to obtain a discrete energy spectrum.

For $l=1$ sometimes a gradient operator with respect to the relative coordinate is used instead of the radial derivative (24). This alternative ansatz reads

$$v_1^{\mathrm{eff}} = \vec{q}\tilde{g}_1 \delta^{(3)}(\vec{r})\vec{q} = \int d^3r |\vec{r}\rangle \overleftarrow{\nabla} \tilde{g}_1 \delta^{(3)}(\vec{r}) \overrightarrow{\nabla} \langle \vec{r}|. \tag{29}$$

It should be noted that the p-wave interaction strength $\tilde{g}_1$ in the gradient formulation is related to the interaction strength (28) by

$$\tilde{g}_1 = g_1/3. \tag{30}$$

3. Beyond scattering length approximation

The operator of the effective contact interaction can be generalized systematically beyond the scattering length approximation shown in the preceding section. A formal scheme emerges from the expansion of the phase shifts in a power series in q

$$\frac{\tilde{\eta}_l(q)}{q^{2l+1}} = \sum_{\nu=0}^{\infty} \frac{1}{\nu!} c_l^{(\nu)} q^{2\nu}. \tag{31}$$

The momentum-independent lowest-order term of this expansion matches the scattering length approximation. From Eq. (21) the connection between the coefficient $c_l^{(0)}$ and the the scattering length a_l becomes obvious

$$c_l^{(0)} = -\frac{(2l+1)}{[(2l+1)!!]^2} a_l^{2l+1}. \tag{32}$$

The coefficient $c_l^{(1)}$ of the quadratic term of the expansion is connected to the so-called effective range or effective volume of the potential. We will discuss this contribution in more detail later. By inserting the expansion (31) into the general formula (20) for the energy shifts we obtain

$$\frac{\Delta E_{nl}}{E_{nl}} = -\frac{2}{\Lambda} \sum_{\nu=0}^{\infty} \frac{1}{\nu!} c_l^{(\nu)} q_{nl}^{2l+2\nu}. \tag{33}$$

Following the basic concept of the ECI these energy shifts have to be generated by the operator of the ECI according to condition (1). To include the momentum dependence of the energy shifts we have to generalize the ansatz for the ECI operator compared to the simple momentum-independent scattering-length formulation (24). The further calculation will show that

$$v_l^{\mathrm{eff}} = \sum_{\nu=0}^{\infty} \tfrac{1}{2} g_l^{(\nu)} [(\vec{q}\cdot\hat{r})^l \delta^{(3)}(\vec{r}) (\hat{r}\cdot\vec{q})^{l+2\nu} + (\vec{q}\cdot\hat{r})^{l+2\nu} \delta^{(3)}(\vec{r}) (\hat{r}\cdot\vec{q})^l] \tag{34}$$

is a proper ansatz for the effective interaction operator for the lth partial wave. Besides the more complex nonlocal structure a set of interaction strengths $g_l^{(\nu)} (\nu = 0,1,\ldots)$ for each partial wave is included. They are related to the coefficients $c_l^{(\nu)}$ and thus correspond to the different powers of the momentum in Eq. (33). To employ condition (1) we calculate the expectation value of v_l^{eff} with noninteracting two-body states $|nlm\rangle$,

$$\begin{aligned} \langle nlm | v_l^{\mathrm{eff}} | nlm \rangle &= \frac{1}{4\pi} \sum_{\nu=0}^{\infty} g_l^{(\nu)} \left[\frac{\partial^l}{\partial r^l} R_{nl}(r) \right]_{r=0} \left[\frac{\partial^{l+2\nu}}{\partial r^{l+2\nu}} R_{nl}(r) \right]_{r=0} \\ &= \frac{A_{nl}^2}{4\pi} \sum_{\nu=0}^{\infty} g_l^{(\nu)} \frac{l!}{(2l+1)!!} \frac{(-1)^\nu (l+2\nu)!}{2^\nu \nu! (2l+2\nu+1)!!} q_{nl}^{2l+2\nu}, \end{aligned} \tag{35}$$

where the full expansion of the noninteracting radial wave function (5) around $r=0$ was used [13]

$$R_{nl}(r) = A_{nl} \sum_{\mu=0}^{\infty} \frac{(-1)^\mu}{2^\mu \mu! (2l+2\mu+1)!!} (q_{nl} r)^{l+2\mu}. \tag{36}$$

By inserting the expansion of the energy shifts (33) and the expectation value into condition (1) and comparing the coefficients for the different powers of the momentum q_{nl} we obtain

$$g_l^{(\nu)} = (-1)^{\nu+1} \frac{4\pi}{2m_{\mathrm{red}}} \frac{2^\nu (2l+1)!! (2l+2\nu+1)!!}{l! (l+2\nu)!} c_l^{(\nu)}. \tag{37}$$

Thus the interaction strengths $g_l^{(\nu)}$ of the general operator form of the ECI (34) are proportional to the coefficients $c_l^{(\nu)}$ of the expansion of the phase shifts (31). Equations (34) and (37) define the most general form of the effective contact interaction.

For the application to dilute degenerate Fermi gases we will use the ECI up to quadratic terms in the momentum, i.e., we include the scattering length term of the s- and p-wave part as well as the s-wave effective range correction. At this point we have to discuss the connection between the qua-

dratic term of the expansion (31) and the usual effective range theory. For the *s*-wave phase shifts the effective range expansion reads

$$q \cot \eta_0(q) \approx -\frac{1}{a_0} + \frac{1}{2} r_0 q^2, \tag{38}$$

where r_0 is the effective range of the potential. If we convert this into an expression for $\tilde{\eta}_0(q)/q$ and expand in q we obtain

$$\frac{\tilde{\eta}_0(q)}{q} = -q_0 - b_0 q^2 + \cdots \tag{39}$$

with an effective volume b_0 that depends on the scattering length a_0 and the effective range r_0

$$b_0 = \tfrac{1}{2} a_0^2 r_0 - \tfrac{1}{3} a_0^3. \tag{40}$$

Rather than using this relation we will adjust b_0 in order to get the best representation of the phase shift $\tilde{\eta}_0(q)/q$ with the truncated expansion (39).

Finally, inserting $c_0^{(1)} = -b_0$ into Eq. (37) gives an expression for the interaction strength of the *s*-wave effective range term

$$g_0^{(1)} = -\frac{12\pi}{2m_{\mathrm{red}}} b_0. \tag{41}$$

C. Example: square-well potential

To illustrate the concept of the effective contact interaction we use the simple toy problem of two particles interacting by an attractive square-well potential of radius λ and depth $-V_0$. First we look at typical wave functions to which the idea of the ECI applies. The major condition is that the typical wavelength of the relative motion is large compared to the range of the interaction. This is ensured by choosing the radius λ of the square well much smaller than the radius Λ associated with the boundary condition (4); in the following we use $\lambda = 0.01\Lambda$. Figure 1 shows the radial wave function of the lowest $l=0$ state with positive energy for different potential depths V_0. Outside the potential the structure of the wave functions is very similar for the different interaction strengths. Only the wavelength is changed slightly due to the different matching to the wave function in the interior (see the inset of Fig. 1). This change of the relative momentum translates immediately into an energy shift. From that picture the connection between energy shifts and phase shifts is evident.

A second point becomes clear from this simple example: The detailed structure of the radial dependence of the potential or the number of bound states is irrelevant for the energy shift, only the phase shifts $\tilde{\eta}_l(q)$ matter. The inset in Fig. 1 shows that the wave functions behave very different within the range λ due to the different potential depths. Moreover, the potentials have a different number of bound states, e.g., the thick solid curve is associated with a potential with one bound state but zero phase shift. Hence the behavior outside the potential is identical to the noninteracting case (thin solid curve) and the energy shift is zero.

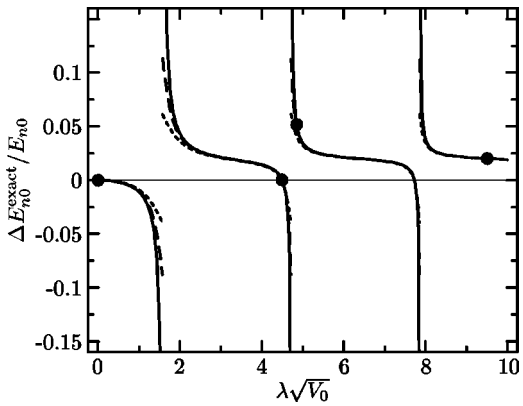

FIG. 3. Relative energy shift $\Delta E_{n0}^{\mathrm{exact}}/E_{n0}$ obtained from the exact $l=0$ solutions plotted versus the strength $\lambda\sqrt{V_0}$ of the square-well potential. The solid line gives the energy shift for the lowest $(n=1)$, the dashed line for the 10th, and the dotted line for the 20th state of the positive-energy spectrum. The dots mark the interaction strengths used in Fig. 1.

Next we investigate the dependence of the $l=0$ energy shifts on the strength of the attractive potential. Figure 3 shows the relative energy shift $\Delta E^{\mathrm{exact}}/E$ versus $\lambda\sqrt{V_0}$, where the radius $\lambda = 0.01\Lambda$ of the square-well potential is kept fixed and the depth V_0 is increased. A characteristic pattern appears: In the vicinity of interaction strengths where the potential gains another bound state the relative energy shift assumes large positive and negative values. Large positive energy shifts occur for potentials that have a very weakly bound state, negative energy shifts for those that have an almost bound state. In between these interaction strengths extended plateaus of nearly constant energy shift appear. Within the plateaus the energy shift is independent of the radial quantum number *n* of the level or the relative momentum. This is a special property of the *s*-wave channel; for higher partial waves the relative energy shift (22) is proportional to q^2[26]. Only at the edges of the plateaus a slight nontrivial dependence on the relative momentum shows up (see Fig. 3).

This structure is closely related to the behavior of the *s*-wave scattering length. The $l=0$ energy shift induced by the ECI in the scattering length approximation (22) is proportional to the scattering length a_0. For the square-well potential we get

$$\frac{\Delta E_{n0}}{E_{n0}} = 2\frac{a_0}{\Lambda} \quad \text{with} \quad \frac{a_0}{\lambda} = 1 - \frac{\tan(\lambda\sqrt{V_0})}{\lambda\sqrt{V_0}}. \tag{42}$$

This ECI energy shift is right on top of the solid curve in Fig. 3, i.e., it agrees very well with the exact energy shift for the lowest positive-energy state. Even for higher momenta the agreement is very good provided that the magnitude of the scattering length is not too large. Significant deviations occur only if momentum *and* scattering length are large.

To obtain a quantitative measure for the applicability of the ECI in the scattering length approximation we investigate the relative deviation $(\overline{E} - \overline{E}^{\mathrm{exact}})/E$ of the ECI energy levels

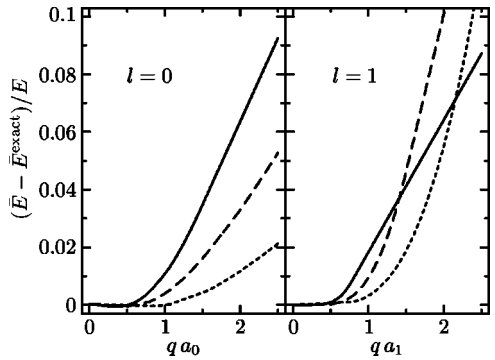

FIG. 4. Relative deviation of the two-body energy calculated with the ECI in scattering length approximation from the exact energy as function of qa_l for $l=0$ (left) and $l=1$ states (right). The curves were obtained for interactions with three bound states by varying the strength $\lambda\sqrt{V_0}$ and looking at the energy shifts for different relative momenta $q_{nl}\Lambda\approx 20$ (solid), 40 (dashed), and 80 (dotted).

compared to the exact ones for the square-well potential. We expect that the agreement gets worse if either the relative momentum or if the scattering length is large. Therefore, Fig. 4 shows the relative energy deviation for $l=0$ and $l=1$ states as a function of the product of momentum and scattering length, qa_l, which was assumed to be small in order to introduce the scattering length (21). The different curves correspond to different values of the momentum q_{nl} and were obtained by varying the depth of the square-well potential and thus the scattering length.

As expected the deviation increases with increasing value of qa_l. Nevertheless, the deviation of the energy calculated with the ECI in the scattering length approximation is below 1% up to rather large values of $qa_l\lesssim 1$. If we tolerate a maximum deviation of 5%, then the scattering length formulation can be used up to values $qa_l\lesssim 1.5$.

It should be noted that the relative deviation of the general form (20) of the ECI in the parameter range discussed above is below 10^{-4}. Thus all approximations made to obtain equation (20) are valid on a high level of accuracy. The restrictions on the validity of the scattering length formulation (22) originate from the replacement of the phase shifts by the scattering length alone, which is not an inherent part of the ECI concept. If the simple scattering length formulation is not sufficient for a special application one can go beyond that.

For example, the inclusion of effective volume corrections [see Eq. (39)] improves the agreement with the exact energy shifts. In this way we can reduce the maximum deviation to only 1% up to $qa_0\lesssim 1.5$.

D. ECI versus pseudopotential

The idea to simulate the effect of a complicated finite-range two-body potential by a simple s-wave contact interaction dates back to Fermi [14] and was used by several authors [15] in various physical contexts. Huang and Yang [16,17] generalized this idea and constructed the so-called *pseudopotential* that acts in all partial waves.

The aim of the pseudopotential is (a) to generate the phase shifts of the original potential by a boundary condition at $r=0$ and (b) to reformulate this by an additional inhomogeneous term in the Schrödinger equation of the two-body scattering problem. This additional term is interpreted as the pseudopotential, which can be phrased in the following operator form [18]:

$$v_l^{\rm pseudo}=\int d^3r|\vec{r}\rangle\frac{1}{r^l}g_l^{\rm pseudo}\delta^{(3)}(\vec{r})\frac{\overrightarrow{\partial}^{2l+1}}{\partial r^{2l+1}}r^{l+1}\langle\vec{r}| \quad (43)$$

with an interaction strength

$$g_l^{\rm pseudo}=\frac{4\pi}{2m_{\rm red}}\frac{(l+1)}{(2l+1)!}a_l^{2l+1} \quad (44)$$

for the lth partial wave. For this discussion we restrict ourselves to the scattering length approximation of the phase shifts. Due to the fact that the radial derivative acts only to the right-hand side the operator of the pseudopotential (43) is not Hermitian. This is in contradiction to the basic concept of effective interactions.

A more severe weakness shows up when we evaluate the energy shifts induced by the pseudopotential. As discussed in Sec. II A the expectation value of a proper effective interaction with eigenstates $|nlm\rangle$ of the noninteracting two-body system should be equal to the energy shift induced by the original potential. For the pseudopotential (43) we obtain an energy shift

$$\frac{\Delta E_{nl}^{\rm pseudo}}{E_{nl}}=\frac{1}{E_{nl}}\langle nlm|v_l^{\rm pseudo}|nlm\rangle$$
$$=\frac{2}{\Lambda}\frac{(l+1)}{[(2l+1)!!]^2}q_{nl}^{2l}\,a_l^{2l+1}. \quad (45)$$

This has to be compared with the full energy shift in scattering length approximation (22) which by construction is reproduced by the ECI. Obviously the energy shift induced by the pseudopotential for states with $l>0$ is by a factor $(l+1)/(2l+1)$ smaller than the energy shift of the original potential. Thus the pseudopotential underestimates the effect of the two-body interactions beyond s-wave when used in a mean-field framework. For the widely used s-wave part the energy shifts of the pseudopotential agree with the energy shifts of the original potential. We conclude that the non-Hermitian pseudopotential is not a proper effective interaction for a mean-field description of dilute quantum gases that goes beyond s-wave interactions.

III. ENERGY FUNCTIONAL OF A TRAPPED MULTICOMPONENT FERMI GAS

A. Fundamentals

In the following we investigate the ground-state properties of a dilute Fermi gas composed of Ξ distinguishable components that are trapped in an external potential $U(\vec{x})$ at temperature $T=0$ K. In the present experiments [2] one or

two components are used, which belong to the same atomic species but are distinguished by different projections M_F of the total angular momentum F onto the direction of an external magnetic field. We distinguish the different components by a formal quantum number $\xi=1,\ldots,\Xi$. For simplicity we use the same mass m of the atoms for all components.

We treat the many-body problem in the framework of density-functional theory and construct an energy functional of the inhomogeneous multicomponent Fermi gas within a proper approximation. The ground-state density distribution of the many-body system is then determined by functional minimization of the energy.

The large particle numbers of the order $N\sim 10^6$ allow the rather simple Thomas-Fermi approximation for the energy functional. It is assumed that the energy density of the inhomogeneous system is described locally by the energy density of the corresponding homogenous system; higher-order terms, which include gradients of the density, are assumed to be small. To check the quality of the Thomas-Fermi approximation we calculated the next order gradient corrections for a trapped noninteracting Fermi gas. For $N=100$ particles the relative contribution of the gradient correction to the total energy is of the order of 10^{-2}; for typical particle numbers of $N=10^6$ it drops to 10^{-5} [18].

As starting point for the Thomas-Fermi approximation we calculate the energy density of the homogenous interacting multicomponent Fermi gas in a mean-field approximation. The basic restriction of the mean-field picture is that two- and many-body correlations induced by the interaction are not contained in the many-body state. Nevertheless they can be implemented implicitly by using a proper effective interaction that is tailored for the model space available. In the preceding section we constructed the effective contact interaction especially for the mean-field description of dilute not-self-bound quantum gases.

A central topic of the following studies is the role of the interaction on the structure and stability of trapped degenerate Fermi gases. Our special interest concerns the p-wave part of the interaction, which contributes even at $T=0$ K—in contrast to bosonic systems. It will turn out that the p-wave terms can be of substantial importance for the ground-state properties of fermionic systems and should not be neglected from the outset.

We write the Hamilton operator of the system as a sum of the external trapping potential U and an internal part $H_{\rm int}$,

$$H=U+H_{\rm int}. \tag{46}$$

The internal part contains the kinetic energy and the effective contact interaction as discussed in Sec. II. We include the s-wave and p-wave terms of the ECI in scattering length formulation as well as the s-wave effective range correction. With Eqs. (24), (28), (34), and (41) the internal Hamiltonian reads

$$\begin{aligned} H_{\rm int}=&\frac{1}{2m}\sum_i \vec{p}_i^{\,2}+\frac{4\pi}{m}a_0\sum_{i,j>i}\delta^{(3)}(\vec{r}_{ij}) \\ &-\frac{12\pi}{m}b_0\sum_{i,j>i}\tfrac{1}{2}[\,\delta^{(3)}(\vec{r}_{ij})(\hat{r}_{ij}\cdot\vec{q}_{ij})^2+\text{H.a.}] \\ &+\frac{12\pi}{m}a_1^3\sum_{i,j>i}(\vec{q}_{ij}\cdot\hat{r}_{ij})\delta^{(3)}(\vec{r}_{ij})(\hat{r}_{ij}\cdot\vec{q}_{ij}). \end{aligned} \tag{47}$$

The summations over the particle indices i and j range from 1 to the total number of particles. The properties of the two-body interaction are parametrized by the s- and p- wave scattering lengths a_0 and a_1, respectively, and by the s-wave effective volume b_0. In general the interaction parameters depend on the component quantum numbers ξ of the interacting particles. In order to discuss the basic phenomena we restrict ourselves to equal interaction parameters for all components. The generalization to scattering length matrices that account for the dependence on the component indices of the two interacting particles is straightforward.

Experimentally each component may experience a different trapping potential $U_\xi(\vec{x})$. For magnetic traps this is due to the different magnetic momenta of the components, which leads to a relative shift of the trapping potentials for the components. Thus the operator of the external potential has the following form:

$$U=\sum_i\sum_\xi U_\xi(\vec{x}_i)\Pi_{\xi,i}, \tag{48}$$

where Π_ξ is a projection operator onto states with the component quantum number ξ.

Many of the results shown in the next sections do not depend on the actual shape of the trapping potential. If the shape enters explicitly we assume a deformed harmonic-oscillator potential

$$\begin{aligned} U(\vec{x})=&\frac{m\omega^2}{2}(\lambda_1^2x_1^2+\lambda_2^2x_2^2+\lambda_3^2x_3^2) \\ =&\frac{1}{2m\ell^4}(\lambda_1^2x_1^2+\lambda_2^2x_2^2+\lambda_3^2x_3^2), \end{aligned} \tag{49}$$

where $\omega=\sqrt[3]{\omega_1\omega_2\omega_3}$ is the mean oscillator frequency and $\ell=(m\omega)^{-1/2}$ the corresponding mean oscillator length i.e., the mean width of the Gaussian single-particle ground state of the harmonic-oscillator potential. The deformation is parametrized by the ratios $\lambda_i=\omega_i/\omega$, which fulfill the condition $\lambda_1\lambda_2\lambda_3=1$.

B. Energy density in the Thomas-Fermi approximation

The calculation of the energy density functional of the inhomogeneous interacting Fermi gas is performed in two steps: First we calculate the energy density of the corresponding homogenous system in the mean-field approximation. In the second step this is translated into an energy density of the inhomogeneous system by means of the Thomas-Fermi approximation.

The ground state of a many-fermion system in mean-field approximation is given by an antisymmetrized product of one-body states $|i\rangle$. In the case of a homogenous system the one-body states are eigenstates of the momentum operator with eigenvalues $\vec{k}_i$. In addition, they are characterized by the component quantum number ξ,

$$|i\rangle = |\vec{k}_i\rangle \otimes |\xi_i\rangle. \tag{50}$$

Assuming a box of volume V with periodic boundary conditions the spatial part of the one-body states is given by

$$\langle \vec{x}|\vec{k}_i\rangle = \frac{1}{\sqrt{V}} \exp(i\vec{k}_i \cdot \vec{x}). \tag{51}$$

The energy density of the homogenous system is given by the expectation value of the internal part of the Hamilton operator (47)

$$\mathcal{E}_{\rm hom} = \langle H_{\rm int}\rangle / V. \tag{52}$$

The calculation of the expectation values of the several parts of the Hamiltonian is straightforward [18]. As a function of the Fermi momenta κ_ξ of the different components the energy density reads

$$\begin{aligned}\mathcal{E}_{\rm hom}(\kappa_1,\ldots,\kappa_\Xi) = {} & \frac{1}{20\pi^2 m}\sum_\xi \kappa_\xi^5 + \frac{a_0}{9\pi^3 m}\sum_{\xi,\xi'>\xi} \kappa_\xi^3 \kappa_{\xi'}^3 \\ & + \frac{a_1^3}{30\pi^3 m}\sum_\xi \kappa_\xi^8 \\ & + \frac{a_1^3 + b_0}{60\pi^3 m}\sum_{\xi,\xi'>\xi} [\kappa_\xi^3 \kappa_{\xi'}^5 + \kappa_\xi^5 \kappa_{\xi'}^3]. \end{aligned} \tag{53}$$

The summations run over all components $\xi = 1,\ldots,\Xi$. To avoid fractional exponents we use Fermi momenta κ_ξ rather than densities $\rho_\xi = \kappa_\xi^3/(6\pi^2)$.

The basic assumption of the Thomas-Fermi (or local-density) approximation is that the energy density of the inhomogenous Fermi gas is locally given by the energy density of the corresponding homogenous system. Thus the energy density of the inhomogeneous system is constructed from Eq. (53) by replacing κ_ξ with *local Fermi momenta* $\kappa_\xi(\vec{x})$. In addition the contribution of the external trapping potential has to be included. This results in the following expression for the energy density of the trapped interacting multicomponent Fermi gas

$$\begin{aligned}\mathcal{E}[\kappa_1,\ldots,\kappa_\Xi](\vec{x}) = {} & \frac{1}{6\pi^2}\sum_\xi U_\xi(\vec{x})\kappa_\xi^3(\vec{x}) + \frac{1}{20\pi^2 m}\sum_\xi \kappa_\xi^5(\vec{x}) \\ & + \frac{a_0}{9\pi^3 m}\sum_{\xi,\xi'>\xi} \kappa_\xi^3(\vec{x})\kappa_{\xi'}^3(\vec{x}) \\ & + \frac{a_1^3}{30\pi^3 m}\sum_\xi \kappa_\xi^8(\vec{x}) \\ & + \frac{a_1^3 + b_0}{60\pi^3 m}\sum_{\xi,\xi'>\xi} [\kappa_\xi^3(\vec{x})\kappa_{\xi'}^5(\vec{x}) \\ & + \kappa_\xi^5(\vec{x})\kappa_{\xi'}^3(\vec{x})]. \end{aligned} \tag{54}$$

The local Fermi momentum is related to the density of particles of the component ξ by

$$\rho_\xi(\vec{x}) = \frac{1}{6\pi^2}\kappa_\xi^3(\vec{x}). \tag{55}$$

Accordingly the number of particles of component ξ is given by

$$N_\xi = \int d^3x \rho_\xi(\vec{x}) = \frac{1}{6\pi^2}\int d^3x \kappa_\xi^3(\vec{x}). \tag{56}$$

As discussed in Sec. II C we can reproduce the two-body energy spectrum with an accuracy of about 5% up to $a_l q \approx 1.5$. If we take this as a limit for the root mean square of the relative momentum $\langle q^2\rangle^{1/2} = 0.53\kappa$ in the many-body system, we can apply our many-body model up to $a_l\kappa \approx 3$.

C. Functional variation and the extremum condition

The ground-state density of a system is found by minimizing the energy functional

$$E[\kappa_1,\ldots,\kappa_\Xi] = \int d^3x \mathcal{E}[\kappa_1,\ldots,\kappa_\xi](\vec{x}) \tag{57}$$

for given particle numbers N_ξ. This constraint is implemented with the help of a set of Lagrange multipliers μ_ξ, which are the chemical potentials of the different components. The Legendre transformed functional

$$\begin{aligned} F[\kappa_1,\ldots,\kappa_\Xi] &= E[\kappa_1,\ldots,\kappa_\Xi] - \sum_\xi \mu_\xi N_\xi \\ &= \int d^3x \mathcal{E}[\kappa_1,\ldots,\kappa_\Xi](\vec{x}) - \sum_\xi \frac{\mu_\xi}{6\pi^2}\kappa_\xi^3(\vec{x}) \\ &= \int d^3x \mathcal{F}[\kappa_1,\ldots,\kappa_\Xi](\vec{x}), \end{aligned} \tag{58}$$

has to be minimized by functional variation. A necessary but not sufficient condition for a set of local Fermi momenta $\{\kappa_1(\vec{x}),\ldots,\kappa_\Xi(\vec{x})\}$ to minimize the transformed energy functional $F[\kappa_1,\ldots,\kappa_\Xi]$ is stationarity, i.e., that the first variation of $F[\kappa_1,\ldots,\kappa_\Xi]$ with respect to all $\kappa_\xi(\vec{x})$ vanishes,

$$\frac{\delta}{\delta\kappa_\xi} F[\kappa_1,\ldots,\kappa_\xi] = 0 \quad \text{for all} \quad \xi. \tag{59}$$

This extremum condition is fulfilled if the derivative of the integrand $\mathcal{F}[\kappa_1,\ldots,\kappa_\Xi](\vec{x})$ with respect to all local Fermi momenta vanishes at each point $(\vec{x})$,

$$\frac{\partial}{\partial\kappa_\xi(\vec{x})}\mathcal{F}[\kappa_1,\ldots,\kappa_\Xi](\vec{x}) = 0 \quad \text{for all} \quad \vec{x},\xi. \tag{60}$$

Inserting expression (54) for the energy density and evaluating the derivative results in the extremum condition

$$m[\mu_\xi - U_\xi(\vec{x})] = \frac{1}{2}\kappa_\xi^2(\vec{x}) + \frac{2a_0}{3\pi}\sum_{\xi'\neq\xi}\kappa_{\xi'}^3(\vec{x}) + \frac{8a_1^3}{15\pi}\kappa_\xi^5(\vec{x}) + \frac{a_1^3+b_0}{30\pi}\sum_{\xi'\neq\xi}[3\kappa_{\xi'}^5(\vec{x}) + 5\kappa_\xi^2(\vec{x})\kappa_{\xi'}^3(\vec{x})] \tag{61}$$

for all $\vec{x}$ and each ξ. This is a coupled set of Ξ polynomial equations for the local Fermi momenta $\{\kappa_1(\vec{x}),\ldots,\kappa_\Xi(\vec{x})\}$ at some given point $\vec{x}$. Note that the trivial solutions $\kappa_\xi(\vec{x})=0$ were separated already. Any real solution of the extremum condition (61) corresponds to a stationary point of the energy functional. In general one has to check explicitly whether they correspond to a minimum of the energy functional or whether they are maxima or saddle points.

All following investigations on the structure and stability of degenerate Fermi gases and on the influence of *s*- and *p*-wave interactions are based on the extremum condition (61). Many physical conclusions can be drawn from its algebraic structure already. We will discuss these questions in detail for the one- and two-component Fermi gas in Secs. IV and V, respectively.

IV. SINGLE-COMPONENT FERMI GAS

As a first application of the formalism developed in Sec. III we study the properties of a degenerate single-component Fermi gas.

A. Effect of the *p*-wave interaction

The energy density of the interacting multicomponent Fermi gas (54) reduces for the single-component system to the form

$$\mathcal{E}[\kappa](\vec{x}) = \frac{1}{6\pi^2}U(\vec{x})\kappa^3(\vec{x}) + \frac{1}{20\pi^2 m}\kappa^5(\vec{x}) + \frac{a_1^3}{30\pi^3 m}\kappa^8(\vec{x}), \tag{62}$$

where $\kappa(\vec{x})$ is the local Fermi momentum. The first term is the contribution of the trapping potential $U(\vec{x})$, the second term is the kinetic energy, and the third term describes the contribution of the *p*-wave interaction with a *p*-wave scattering length a_1. As mentioned earlier the *s*-wave part of the interaction does not contribute in a system of identical fermions due to the Pauli principle. Therefore the *p*-wave part is the leading interaction term and there is no reason to neglect it from the outset.

A first hint on the effects of the *p*-wave interaction is given by the density distributions for different values of the *p*-wave scattering length. The density distribution is obtained by the solution of the extremum condition (61), which takes the simple form

$$m[\mu - U(\vec{x})] = f_1[\kappa(\vec{x})]$$

with

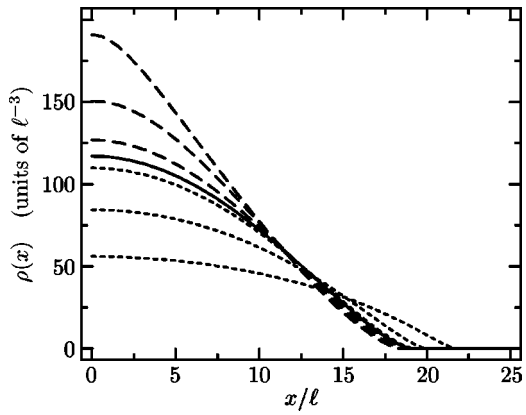

FIG. 5. Density profile $\rho(x)$ of a single-component Fermi gas of $N=10^6$ particles trapped in a spherical symmetric parabolic trap with oscillator length ℓ. The solid curve shows the noninteracting gas $a_1/\ell=0$. Dotted curves correspond to repulsive *p*-wave interactions with $a_1/\ell=0.03$, 0.06, and 0.1 (from top to bottom). The dashed curves show attractive *p*-wave interactions with $a_1/\ell=0.03$, -0.04, and -0.044 (top to bottom), respectively.

$$f_1(\kappa) = \frac{1}{2}\kappa^2 + \frac{8a_1^3}{15\pi}\kappa^5. \tag{63}$$

This fifth-order polynomial equation for the local Fermi momentum $\kappa(\vec{x})$ is solved numerically for each point $\vec{x}$. The chemical potential μ is adjusted such that particle number (56) assumes the desired value.

Figure 5 shows the resulting radial density profiles $\rho(x)=\kappa^3(x)/(6\pi^2)$ for a single-component gas of $N=10^6$ particles in a spherical trap with oscillator length ℓ for different *p*-wave scattering lengths a_1. The oscillator length defines the fundamental length scale of the problem and the parameter that determines the strength of the interaction is the ratio of the *p*-wave scattering length and oscillator length, a_1/ℓ. To increase the magnitude of this ratio experimentally one can either increase the magnitude of the scattering length or decrease the oscillator length.

For a repulsive *p*-wave interaction, i.e., $a_1/\ell>0$, of increasing strength (dotted curves) the density distribution flattens and expands radially compared to the noninteracting system (solid line). For a ratio $a_1/\ell=0.1$ the central density has dropped to one-half of the density of the noninteracting gas. With a typical experimental oscillator length of $\ell=1\,\mu$m this ratio corresponds to a rather large scattering length of $a_1\approx 2000a_B$, which nevertheless may be within the range of experimental parameters [8]. For a tightly confining trap with $\ell=0.1\,\mu$m a moderate scattering length of $a_1\approx 200a_B$ is required to obtain the same ratio.

For an attractive *p*-wave interaction, $a_1/\ell<0$, the central density increases significantly with increasing interaction strength. If the central density exceeds a certain value or if $|a_1/\ell|$ exceeds a critical value, then the extremum condition (63) has no real solution any more. Physically this corresponds to a collapse of the dilute gas caused by the attractive mean-field that is generated by the *p*-wave interaction. We will discuss this question in detail in the following sections. The dependence of the density distribution on the *p*-wave

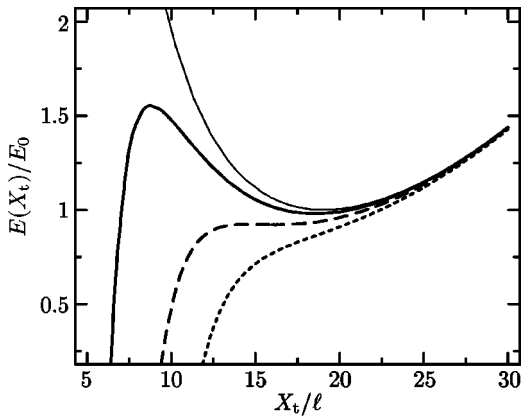

FIG. 6. Variational energy (65) of a trapped single-component Fermi gas with $N=10^6$ as a function of the parameter X_t. The curves show the noninteracting gas (thin solid), $a_1/\ell=-0.035$ (solid), $a_1/\ell=-0.051$ (dashed), and $a_1/\ell=-0.065$ (dotted). The energies are given in units of the ground-state energy E_0 of the noninteracting gas.

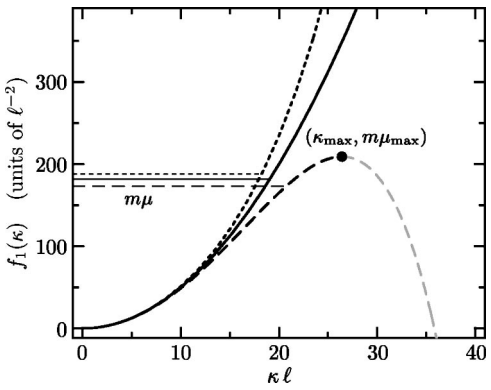

FIG. 7. Right-hand side $f_1(\kappa)$ of the extremum condition (63) as a function of the Fermi momentum for a noninteracting singe-component gas (solid) with repulsive p-wave interaction $a_1/\ell=-0.04$ (dotted) and with attractive p-wave interaction $a_1/\ell=-0.04$ (dashed). The horizontal lines mark the respective values of the chemical potentials for $N=10^6$ particles.

scattering length as depicted in Fig. 5 already demonstrates that the p-wave interaction may have strong influence on the properties of degenerate Fermi gases.

B. Mean-field instability: a variational picture

To illustrate the origin and mechanism of the collapse of the metastable state of the trapped Fermi gas we utilize a simple variational picture. Assume a single-component Fermi gas of N particles in a spherical symmetric oscillator potential. The local Fermi momentum of the interacting system is parametrized by the analytic expression for the local Fermi momentum of the noninteracting system

$$\kappa(\vec{x})=\frac{2(6N)^{1/3}}{X_t}\sqrt{1-\left(\frac{|\vec{x}|}{X_t}\right)^2}\quad\text{for}\quad|\vec{x}|\leqslant X_t, \tag{64}$$

where the classical turning point X_t is treated as variational parameter. By inserting this parametrization into the energy density (62) and integrating we obtain a closed expression for the energy as function of the parameter X_t

$$E(X_t)=C_u\frac{NX_t^2}{\ell^4}+C_t\frac{N^{5/3}}{X_t^2}+C_1\frac{N^{8/3}a_1^3}{X_t^5}, \tag{65}$$

with constant coefficients

$$C_u=\frac{3}{16m},\quad C_t=\frac{3(9/2)^{1/3}}{2m},\quad C_1=\frac{8^6(4/3)^{1/3}}{1925\pi^2 m}. \tag{66}$$

Again the first term corresponds to the external potentials, the second to the kinetic energy, and the third term to the p-wave interaction.

Figure 6 shows the dependence of the total energy (65) on the parameter X_t for a system of $N=10^6$ particles with different p-wave scattering lengths. For attractive p-wave interactions, i.e., negative scattering length a_1, the contribution of the interaction in Eq. (65) is negative. Due to its X_t^{-5} dependence this interaction contribution leads to a rapid drop of the energy for systems of decreasing spatial extension and thus increasing density. At very high densities (small X_t) one formally ends up with states of negative energy, i.e., bound states. One should, however, keep in mind that the assumptions made for the construction of the effective contact interaction are not valid in this high-density regime anymore.

The not-self-bound metastable state appears as local minimum at positive energies and low densities provided the p-wave attraction is sufficiently weak; the thick solid curve in Fig. 6 shows an example. If the strength of the attractive p-wave interaction increases, then the local minimum flattens and devolves to a saddle point (dashed curve). From this particular interaction strength on the metastable low-density state does not exist anymore, only the true ground state of the system remains, which is usually a crystal. The system collapses if the barrier caused by the positive kinetic and the attractive mean-field energy vanishes. Since the mean-field attraction grows with increasing density the system is unstable and collapses towards a high-density configuration.

C. Mean-field instability: stability conditions

Based on the extremum condition (63) we derive a set of analytic stability conditions that relate the maximum density of a metastable system with the p-wave scattering length. Part of this was already discussed in [10].

The mean-field instability of the system occurs for values of the chemical potential μ and the scattering length a_1, where the extremum condition (63) does not have a real solution anymore. This is shown in a pictorial way in Fig. 7 where the right-hand side $f_1(\kappa)$ of the extremum condition is plotted as function of κ for different a_1/ℓ. The solution of the extremum condition at some specific point $\vec{x}$ is given by the value of κ at which the respective curve reaches the value $m[\mu-U(\vec{x})]$. In the minimum of the trapping potential [we assume $U(\vec{x})=0$ in the minimum] the solution is given by the point where $f_1(\kappa)$ reaches the value $m\mu$. By moving towards the outer regions of the trap $m[\mu-U(\vec{x})]$ decreases

and one scans $f_1(\kappa)$ down along ordinate until one reaches $m[\mu - U(\vec{x})] = 0$, i.e., the classical turning point.

For repulsive *p*-wave interactions (dotted curve) the rhs of Eq. (63) is a monotonic growing function and solutions exist for arbitrary values of $m[\mu - U(\vec{x})]$. If the scattering length a_1 is negative (dashed curve), then $f_1(\kappa)$ exhibits a maximum at a Fermi momentum $\kappa_{\max}$ and chemical potential $\mu_{\max}$

$$\kappa_{\max} = -\frac{\sqrt[3]{3\pi}}{2a_1}, \quad \mu_{\max} = \frac{3(3\pi)^{2/3}}{40ma_1^2}. \tag{67}$$

For values of the chemical potential $\mu > \mu_{\max}$ no solution of the extremum condition exists, i.e., there is no metastable low-density state. Equivalently only solutions with local Fermi momenta below $\kappa_{\max}$ correspond to minima of the energy functional; those above $\kappa_{\max}$ (gray segment of the dashed curve) correspond to maxima of the energy. Thus we get a limiting condition for the local Fermi momentum of the metastable state

$$-a_1\kappa(\vec{x}) \leqslant \frac{\sqrt[3]{3\pi}}{2} \tag{68}$$

or in terms of the density

$$-a_1^3\rho(\vec{x}) \leqslant \frac{1}{16\pi}. \tag{69}$$

This is one form of the *stability condition* for the single-component Fermi gas. We note that this condition is completely independent of the trap geometry. As soon as the stability condition is violated somewhere in the trap, in general in the minimum of the trapping potential, the system will become unstable.

For practical purposes we formulate a stability condition in terms of the particle number *N*. The maximum particle number $N_{\max}$ of the metastable degenerate Fermi gas is directly connected to the maximum chemical potential $\mu_{\max}$. This relation is established numerically by solving the extremum condition for the maximum chemical potential $\mu_{\max}$ and integrating over the resulting density distribution to obtain the corresponding maximum particle number (56). This is done for several scattering lengths a_1 assuming a deformed oscillator potential (49) with mean oscillator length ℓ. Finally a parametrized form of the stability condition is fitted to this data. The parametrization is motivated by the noninteracting gas, where the maximum local Fermi momentum is proportional to $\sqrt[6]{N}/\ell$. Inserting this into the stability condition (68) leads to the form

$$C\left(\sqrt[6]{N}\frac{a_1}{\ell}\right) \leqslant 1, \quad C = -2.246. \tag{70}$$

The parameter *C* is fitted to the numerical results, which are reproduced with a deviation far below 1%. Note that this condition is independent of the deformation of the harmonic-oscillator trap [18].

For an interaction strength of $a_1/\ell = -0.01$ which corresponds to a scattering length $a_1 \approx -200a_B$ for a trap with $\ell = 1\,\mu$m the maximum particle number is $N_{\max} = 7.8 \times 10^9$. This seems to be out of the range of present experiments. Nevertheless if we increase the strength of the *p*-wave attraction to $a_1/\ell = -0.1$, then the maximum particle number drops to $N_{\max} = 7800$. Experimentally this could be achieved by utilizing a *p*-wave Feshbach resonance to increase the *p*-wave scattering length to $a_1 \approx -2000a_B$ as proposed by Bohn [8] for the ^{40}K system.

V. TWO-COMPONENT FERMI GAS

As a second application we consider the degenerate two-component Fermi gas.

A. Interplay between the *s*- and *p*-wave interaction

The general energy density of a trapped multicomponent Fermi gas in the Thomas-Fermi approximation (54) takes for the two-component system the following form:

$$\begin{aligned}\mathcal{E}[\kappa_1,\kappa_2](\vec{x}) = {} & \frac{1}{6\pi^2}[U_1(\vec{x})\kappa_1^3(\vec{x}) + U_2(\vec{x})\kappa_2^3(\vec{x})] \\ & + \frac{1}{20\pi^2 m}[\kappa_1^5(\vec{x}) + \kappa_2^5(\vec{x})] \\ & + \frac{a_0}{9\pi^3 m}\kappa_1^3(\vec{x})\kappa_2^3(\vec{x}) \\ & + \frac{a_1^3}{30\pi^3 m}[\kappa_1^8(\vec{x}) + \kappa_2^8(\vec{x})] \\ & + \frac{a_1^3 + b_0}{60\pi^3 m}[\kappa_1^3(\vec{x})\kappa_2^5(\vec{x}) + \kappa_1^5(\vec{x})\kappa_2^3(\vec{x})],\end{aligned} \tag{71}$$

where $\kappa_1(\vec{x})$ and $\kappa_2(\vec{x})$ denote the local Fermi momenta of the two components. In contrast to the single-component system, both *s*- and *p*-wave terms of the effective contact interaction contribute. The *s*-wave interaction acts only between particles of different species and generates a contribution proportional to the product of the densities of both components. The *p*-wave term acts between particles of different components as well as between particles of the same species. For reasons of simplicity we assume the same *p*-wave scattering length a_1 for these different interactions.

Including the constraint of given particle numbers N_1 and N_2 of the two components with the help of the chemical potentials μ_1 and μ_2 (see Sec. III C) leads to the transformed energy density

$$\mathcal{F}[\kappa_1,\kappa_2](\vec{x}) = \mathcal{E}[\kappa_1,\kappa_2](\vec{x}) - \frac{\mu_1}{6\pi^2}\kappa_1^3(\vec{x}) - \frac{\mu_2}{6\pi^2}\kappa_2^3(\vec{x}). \tag{72}$$

Functional variation of the transformed energy functional leads to the extremum condition. For the two-component system the general form (61) reduces to a coupled set of two polynomial equations

$$m[\mu_1 - U_1(\vec{x})] = \frac{1}{2}\kappa_1^2(\vec{x}) + \frac{2a_0}{3\pi}\kappa_2^3(\vec{x}) + \frac{8a_1^3}{15\pi}\kappa_1^5(\vec{x}) + \frac{a_1^3 + b_0}{30\pi}[3\kappa_2^5(\vec{x}) + 5\kappa_1^2(\vec{x})\kappa_2^3(\vec{x})], \tag{73}$$

where the second equation is generated by the exchange $\kappa_1(\vec{x}) \leftrightarrow \kappa_2(\vec{x})$ and $[\mu_1 - U_1(\vec{x})] \rightarrow [\mu_2 - U_2(\vec{x})]$. Trivial solutions with $\kappa_1(\vec{x}) = 0$ and $\kappa_2(\vec{x}) = 0$, respectively, are already separated in this expression.

These coupled equations have a great variety of solutions. In order to show the generic phenomena of the two-component system without too many parameters we restrict ourselves to equal numbers of particles in both components $N = N_1 = N_2$ as well as trapping potentials that differ only by an additive constant, thus $\mu - U(\vec{x}) = \mu_1 - U_1(\vec{x}) = \mu_2 - U_2(\vec{x})$.

We will concentrate the further studies on the stability of the degenerate two-component Fermi gas against mean-field collapse. For this phenomenon solutions with identical local Fermi momenta for both components, $\kappa(\vec{x}) = \kappa_1(\vec{x}) = \kappa_2(\vec{x})$, are relevant. Under this assumption the extremum condition reduces to a single equation

$$m[\mu - U(\vec{x})] = f_2[\kappa(\vec{x})] \tag{74}$$

with

$$f_2(\kappa) = \frac{1}{2}\kappa^2 + \frac{2a_0}{3\pi}\kappa^3 + \frac{4\tilde{a}_1^3}{5\pi}\kappa^5.$$

For simplicity we introduce a modified p-wave scattering length[2]

$$\tilde{a}_1^3 = a_1^3 + b_0/3, \tag{75}$$

which contains the s-wave effective volume parameter. In the following we will discuss the properties of the two-component Fermi gas as function of the s-wave and the modified p-wave scattering length.

For other phenomena, like the separation of the two components due to repulsive interactions, different classes of solutions become important. We will discuss these in a future publication.

B. Mean-field instability: stability conditions

The stability of the two-component Fermi gas under the influence of s- and p-wave interactions can be investigated with tools similar to the single-component case. Here the solutions with identical Fermi momenta for both components are of interest.

Similar to the single-component case the right-hand side $f_2(\kappa)$ of the extremum condition (74) may exhibit a maximum if the s-wave or the p-wave scattering length is negative. Thus the density and particle number of the metastable low-density state may be limited. For a detailed analysis one has to look at all possible combinations of signs of the s- and p-wave scattering lengths separately.

$a_0 \geqslant 0$, $\tilde{a}_1 \geqslant 0$. For a purely repulsive interaction $f_2(\kappa)$ is a monotonic growing function and no mean-field induced collapse occurs.

$a_0 < 0$, $\tilde{a}_1 \leqslant 0$. For purely attractive interactions $f_2(\kappa)$ shows a maximum; thus the density of the metastable low-density state is limited.

$a_0 \geqslant 0$, $\tilde{a}_1 < 0$. The negative contribution of the p-wave interaction dominates $f_2(\kappa)$ at high densities and generates a maximum, i.e., the mean-field induced collapse can occur even if the s-wave interaction is repulsive.

$a_0 < 0$, $\tilde{a}_1 > 0$. It depends on the relative strength of the s- and p-wave interaction whether the rhs of the extremum condition has a local maximum or grows monotonically.
Especially the stability in the last case depends on a subtle competition between s- and p-wave interactions. Moreover, it shows some completely new phenomena, which will be discussed in the following section.

For those cases where $f_2(\kappa)$ has a maximum the value of the local Fermi momentum $\kappa_{\max}$ at the maximum is given by the equation

$$-a_0\kappa_{\max} - 2[\tilde{a}_1\kappa_{\max}]^3 = \frac{\pi}{2}. \tag{76}$$

Again $\kappa_{\max}$ is an upper limit for the local Fermi momenta, which can occur for a metastable low-density state of the two-component gas. Thus we can formulate the stability condition

$$-a_0\kappa(\vec{x}) - 2[\tilde{a}_1\kappa(\vec{x})]^3 \leqslant \frac{\pi}{2} \tag{77}$$

or equivalently in terms of the density

$$-[6\pi^2 a_0^3 \rho(\vec{x})]^{1/3} - 12\pi^2\tilde{a}_1^3\rho(\vec{x}) \leqslant \frac{\pi}{2}. \tag{78}$$

If these stability conditions are violated, then no metastable low-density state exists for the two-component Fermi gas. For a pure s-wave interaction ($\tilde{a}_1 = 0$) the stability condition (77) reduces to the form $-a_0\kappa(\vec{x}) \leqslant \pi/2$, which was obtained earlier by Houbiers *et al.* [5]. Compared to this simple form the inclusion of the p-wave interaction reveals several new effects.

Before we discuss the structure of Eq. (77) we formulate an equivalent stability condition in terms of the number of particles $N = N_1 = N_2$ of each component. For given values of the two scattering lengths the maximum local Fermi momentum and the maximum chemical potential is calculated.

[2]This can be generalized to include different p-wave scattering lengths for the different combinations of the two species: $\tilde{a}_1^3 = \frac{1}{3}(a_{1[11]}^3 + a_{1[22]}^3 + a_{1[12]}^3 + b_0)$.

TABLE I. Parameters of the fitted stability condition (79) for the two-component Fermi gas for different interaction types.

Interaction type	C_0	C_1	C_{01}	n
$a_0 \leqslant 0,\ \tilde{a}_1 \leqslant 0$	-1.835	-2.570	0.656	1
$a_0 \geqslant 0,\ \tilde{a}_1 < 0$	-1.378	-2.570	1.360	1
$a_0 < 0,\ \tilde{a}_1 \leqslant 0$	-1.835	-1.940	2.246	3

From the solution of the extremum condition (74) for these parameters the corresponding maximum particle number is determined. These numerical data are fitted by a suitable parametrization of the stability condition in terms of the particle number and the scattering lengths a_0/ℓ and $\tilde{a}_1/\ell$

$$C_0\left(\sqrt[6]{N}\frac{a_0}{\ell}\right)+C_1^3\left(\sqrt[6]{N}\frac{\tilde{a}_1}{\ell}\right)^3+C_{01}^{n+1}\left(\sqrt[6]{N}\frac{a_0}{\ell}\right)\left(\sqrt[6]{N}\frac{\tilde{a}_1}{\ell}\right)^n \leqslant 1. \tag{79}$$

This parametrization is constructed in analogy to the single-component case (70); the additional cross-term is necessary to achieve a similar accuracy with typical deviations below 1%. The parameters C_0, C_1, and C_{01} have to be fitted for each combination of signs of the two scattering lengths separately. The value of n is not included in the fitting procedure but chosen by hand. The resulting values are summarized in Table I.

Figure 8 illustrates the dependence of the maximum particle number resulting from this stability condition on the *s*- and *p*-wave scattering lengths. The contour plot shows the logarithm of the maximum particle number for each component as function of a_0/ℓ and $\tilde{a}_1/\ell$. The first gross observation is that attractive *s*- and *p*-wave interactions with similar scattering lengths set similar restrictions to the stability of the two-component Fermi gas. For example, a pure *s*-wave interaction with $a_0/\ell=-0.05$ leads to a maximum particle number of $N_{\max}\approx 1.7\times 10^6$. In comparison a pure *p*-wave

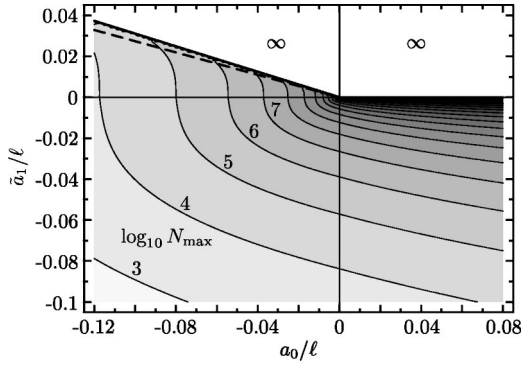

FIG. 8. Contour plot of the logarithm of the maximum particle number, $\log_{10} N_{\max}$, as a function of the *s*-and *p*-wave scattering lengths for a two-component Fermi gas in a harmonie-oscillator potential with mean oscillator length ℓ. Selected contours are labeled with the corresponding value of $\log_{10} N_{\max}$. In the white area at a positive *p*-wave scattering length no collapse can occur, i.e., the maximum particle number is infinity.

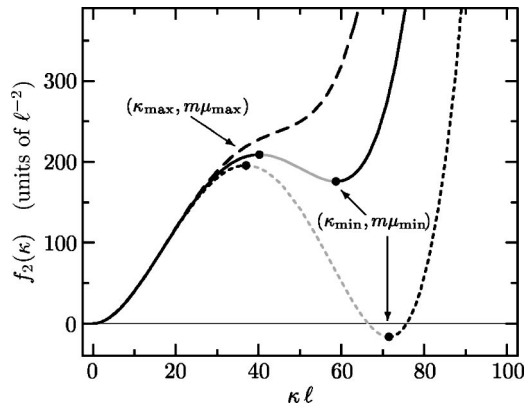

FIG. 9. Right-hand side $f_2(\kappa)$ of the extremum condition (74) as a function of the Fermi momentum for an attractive *s*-wave interaction with $a_0/\ell=-0.05$ and a repulsive *p*-wave interaction with $\tilde{a}_1/\ell=0.014$ (dotted curve), 0.015 (solid), and 0.016 (dashed). The gray segments of the curves correspond to the maxima of the energy density.

interaction with the same scattering length $\tilde{a}_1/\ell=-0.05$ causes a collapse at even lower particle numbers of $N_{\max}\approx 2.2\times 10^5$.

If both interaction parts are attractive they cooperate and cause an instability at lower particle numbers or densities. If the interaction is attractive in one partial wave and repulsive in the other, then the repulsive part leads to a stabilization, i.e., it increases the maximum particle number. Here a significant difference between *s*- and *p*-wave interactions arises: The stabilization caused by a repulsive *s*-wave interaction is rather weak. Compared to a pure *p*-wave interaction with $\tilde{a}_1/\ell=-0.05$ the presence of a *s*-wave repulsion of the same magnitude $a_0/\ell=0.05$ increases the maximum particle number only from 2.2×10^5 to 8.9×10^5. In the opposite case of an attractive *s*-wave interaction a *p*-wave repulsion of the same magnitude will always lead to an absolute stabilization, i.e., there is no collapse for an arbitrary large particle number despite the *s*-wave attraction. We will study these special effects in detail in the following section.

We should like to point out that for strong repulsive *s*-wave interactions the system can gain energy by seperating the two components spatially. This demixing phenomenon will be discussed in a future paper.

These results clearly demonstrate that it is necessary to include the *p*-wave interaction if the scattering length $\tilde{a}_1$ is roughly in the same order of magnitude as the *s*-wave scattering length. Even if the ratio of the scattering lengths, $\tilde{a}_1/a_0$, are approximately 0.3 dramatic effects like the *p*-wave stabilization, which is discussed in Sec. V C, can occur. As can be seen from Fig. 8 the *p*-wave interaction may be neglected only if the ratio $\tilde{a}_1/a_0$ is smaller than 0.1.

C. Mean-field instability: *p*-wave stabilization

Several phenomena occur due to the competition between an attractive *s*-wave ($a_0<0$) and a repulsive *p*-wave interaction ($\tilde{a}_1>0$). To understand the origin of these phenomena, which are a unique property of these type of interactions, we

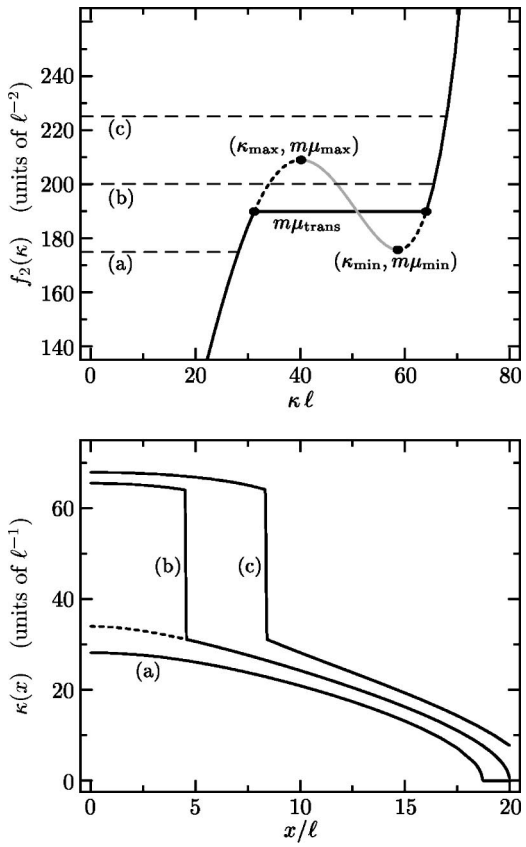

FIG. 10. Upper plot: $f_2(\kappa)$ of the extremum condition (74) as a function of the Fermi momentum for an interaction with $a_0/\ell = -0.05$ and $\tilde{a}_1/\ell = 0.015$. Lower plot: Distribution of local Fermi momenta $\kappa(x)$ for a spherical trap of oscillator length ℓ for the three different chemical potentials marked in the upper panel. Solid curves show the equilibrium profiles, dotted curves show metastable configurations.

investigate the right-hand side $f_2(\kappa)$ of the extremum condition (74). Figure 9 depicts the dependence of $f_2(\kappa)$ on the local Fermi momentum for an s-wave scattering length $a_0/\ell = -0.05$ and three slightly different positive p-wave scattering lengths in the range $a_0/\ell = 0.014, \ldots, 0.016$.

Due to the dominant κ^5 dependence any repulsive p-wave interaction causes $f_2(\kappa)$ to grow fast for large Fermi momenta. Thus the maximum is only local and does not determine necessarily the maximum Fermi momentum or chemical potential as in the cases with attractive or vanishing p-wave interaction. If the p-wave repulsion is sufficiently strong the local maximum vanishes completely and $f_2(\kappa)$ is a monotonically growing function. In this case a solution of the extremum condition exists for any density, chemical potential, or particle, number. An example is shown by the dashed curve in Fig. 9. It can be seen from Eq. (74) that the local maximum disappears if the ratio of the two scattering lengths fulfills the condition

$$\frac{\tilde{a}_1}{|a_0|} \geqslant \frac{2}{3\pi^{2/3}} \approx 0.311. \tag{80}$$

If this condition is fulfilled the p-wave repulsion causes an *absolute stabilization* of the system against s-wave induced collapse. In this case the total mean-field contribution of the interactions is always repulsive and grows monotonically with density.

Notice that the p-wave scattering length necessary for this stabilization is only approximately 1/3 of the modulus of the s-wave scattering length. Obviously the p-wave interaction may have drastic influence on the stability even if it is significantly weaker than the s-wave interaction in terms of scattering lengths.

For weaker p-wave repulsions $f_2(\kappa)$ still shows a local maximum and in addition a (local) minimum at larger Fermi momenta. Examples are shown by the solid and dotted curves in Fig. 9. In this case the extremum condition has two branches that correspond to local minima of the energy density, which are separated by a branch of local maxima (gray segments). The branch at lower Fermi momenta corresponds to the usual family of low-density solutions that were obtained with other types of interactions too. It ends up at the local maximum with $\kappa_{\max}$ given by Eq. (76) and $m\mu_{\max} = f_2(\kappa_{\max})$. The solution branch at higher Fermi momenta gives rise to a new family of high-density solutions, which are unique for this type of interaction. It is bounded from below by the local minimum $(\kappa_{\min}, \mu_{\min})$ and raises up to arbitrary Fermi momenta and chemical potentials.

For values of $[\mu - U(\vec{x})]$ between $\mu_{\min}$ and $\mu_{\max}$ the extremum condition has two solutions κ_{low} and κ_{high} with $f_2(\kappa_{\text{low}}) = f_2(\kappa_{\text{high}})$, see Fig. 10. In equilibrium the one with lower energy density (72) is realized. We define a chemical potential μ_{trans} at which the energy densities of both branches are equal; the value of μ_{trans} can be determined numerically. Since we expect the solution $\kappa(\vec{x})$ to correspond to a minimum of the energy functional at each point $\vec{x}$, for $[\mu - U(\vec{x})] < \mu_{\text{trans}}$ the low-density branch gives the equilibrium solution and for $[\mu - U(\vec{x})] > \mu_{\text{trans}}$ the high-density branch does. This gives rise to a Maxwell construction for the rhs of the extremum condition (74) as illustrated in the upper plot of Fig. 10. The dotted parts of the lower and upper branch in Fig. 10 correspond to local minima and may occur as metastable states that eventually undergo a transition to the energetically lower equilibrium solution.

The structure of the density distribution depends crucially on the value of the chemical potential μ, i.e., the particle number. The upper plot of Fig. 10 shows the rhs of the extremum condition (74) for an interaction with $a_0/\ell = -0.05$ and $\tilde{a}_1/\ell = 0.015$. The dashed horizontal lines mark three different chemical potentials. The lower plot shows the radial dependencies of the local Fermi momenta $\kappa(x) = (6\pi^2\rho(x))^{1/3}$ for these three chemical potentials assuming a spherical trap with oscillator length ℓ. For chemical potentials $\mu < \mu_{\text{trans}}$—case (a) in Fig. 10—the equilibrium solution is completely on the low-density branch and we obtain the usual smooth density profile. If $\mu > \mu_{\text{trans}}$—cases (b) and (c) in Fig. 10—then the equilibrium solution in the center of the trap is given by the high-density branch, while the solution for the outer regions of the trap is given by the low-density branch. Thus the equilibrium density profile shows a jump in density by typically one order of magnitude as one approaches the center of the trap. The location of the discontinuity is always given by the equation $[\mu - U(\vec{x})] = \mu_{\text{trans}}$

which reflects the mechanical equilibrium between the low- and the high-density phase, i.e., the equality of the pressures $p=-\mathcal{F}[\kappa](\vec{x})$ at the boundary between the two phases.

If the chemical potential is still below $\mu_{\max}$—case (b) in Fig. 10—then a solution with a smooth low-density profile all over the trap may exist as a metastable state. Due to density fluctuations this state may undergo a transition to the energetically preferred equilibrium state, which includes the high-density phase.

The physical origin of the high-density phase is quite intuitive: The usual stability is determined by a competition between the kinetic energy, which favors low densities, and the attractive mean field, which prefers higher densities. If the attractive mean field becomes too strong, then the kinetic energy is not able to stabilize the system anymore and the mean-field collapse occurs. In case of the high-density phase the attractive mean field generated by the *s*-wave interaction has already overcome the stabilizing effect of the kinetic energy. Nevertheless the collapse is prevented by the repulsive *p*-wave contribution, which grows for higher densities faster than the *s*-wave attraction and inhibits a further increase of density. We call this remarkable phenomenon the *p-wave stabilized high-density phase*—in contrast to the low-density phase stabilized by the kinetic energy, which is still present in the peripheral regions of the trap.

The situation discussed so far assumes a repulsive *p*-wave interaction that is slightly too weak to cause the absolute stabilization according to Eq. (80). If the *p*-wave strength is decreased further, then the values of $\mu_{\min}$, $\mu_{\max}$, and μ_{trans} also decrease. If the ratio of the *p*-wave and *s*-wave scattering lengths drops below the limit

$$\frac{\tilde{a}_1}{|a_0|}<\sqrt[3]{\frac{160}{729\pi^2}}\approx 0.281, \tag{81}$$

then the chemical potential of the minimum is negative, $\mu_{\min}<0$. An example is shown by the dotted curve in Fig. 9. For even weaker *p*-wave interactions with

$$\frac{\tilde{a}_1}{|a_0|}<0.274, \tag{82}$$

μ can be negative. That means that the high-density solution forms a self-bound state independent of the trapping potential. Therefore as soon as the maximum chemical potential $\mu_{\max}$ is exceeded the gas collapses into a self-bound high-density state which is independent of the trap.

We summarize the variety of structures that appear for interactions with an attractive *s*-wave ($a_0<0$) and repulsive *p*-wave part ($\tilde{a}_1>0$) in the following list.

$0.311<\tilde{a}_1/|a_0|$. The *p*-wave repulsion stabilizes the system for arbitrary densities and particle numbers with a smooth low-density profile. For ratios of the scattering lengths near the limit a smooth but significant increase of the central density occurs.

$0.274<\tilde{a}_1/|a_0|<0.311$. For chemical potentials below $\mu_{\max}$ or particle numbers below the corresponding maximum particle number (79) the usual low-density solution exists.

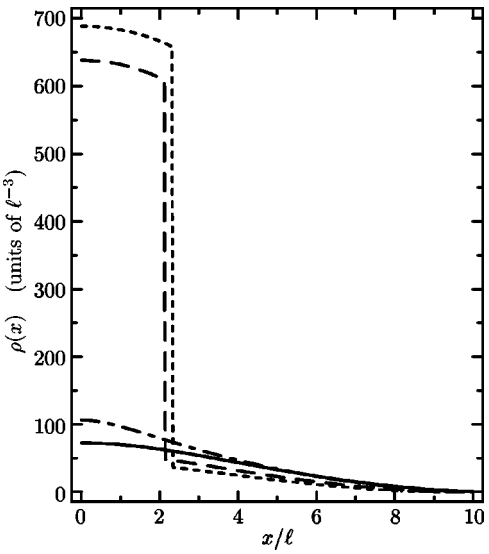

FIG. 11. Evolution of the density profile of a two-component system of $N=N_1=N_2=60\,000$ particles with a *p*-wave scattering length $\tilde{a}_1/\ell=0.03$ according to the *Gedankenexperiment* described in the text. The *s*-wave scattering length is tuned in the range $a_0/\ell=-0.095$ (solid), -0.1 (dash-dotted), -0.101 (dashed), and -0.102 (dotted).

Above these values the *p*-wave stabilized high-density phase appears, i.e., the density in the central region of the trap is increased by typically one order of magnitude compared to the low-density profile in the outer regions.

$\tilde{a}_1/|a_0|<0.274$. Below $\mu_{\max}$ or $N_{\max}$ a stable solution with the regular low-density profile exists. Above the system collapses; the high-density phase is not stable anymore.

This subtle dependence on the ratio of the scattering lengths is illustrated in Fig. 8. The white region for ''strong'' repulsive *p*-wave interactions shows the domain of absolute stabilization. The solid line corresponds to the condition (80) for absolute stabilization, the dashed line to condition (82) for the stability of the high-density phase. The small area between those lines represents the parameter region where the *p*-wave stabilized high-density phase exists if the maximum particle number is exceeded.

To conclude this section we perform a *Gedankenexperiment:* Assume a two-component Fermi gas of $N=N_1=N_2=60\,000$ particles in each component trapped in a spherical oscillator potential with $\ell=1\,\mu$m. May the interaction be composed of a repulsive *p*-wave part with $\tilde{a}_1/\ell=0.03$ and an attractive *s*-wave component that can be tuned within a small range $a_0/\ell=-0.095,\ldots,-0.102$, e.g., by using a Feshbach resonance. Figure 11 shows the evolution of the density profile of the Fermi gas if the strength of the attractive *s*-wave interaction is increased slowly such that density fluctuations are negligible. For $a_0/\ell=-0.095$ (solid curve) and -0.1 (dash-dotted) we observe a smooth low-density profile, where the central density increases slightly with increasing *s*-wave attraction. A dramatic change happens if the attraction is increased to $a_0/\ell=-0.101$ (dashed). For this interaction strength the particle number of the system is already above the maximum particle number given by Eq. (79)

and the high-density phase appears and occupies a rather large volume. A further increase of the s-wave attraction (dotted) causes a growth of the high-density phase. If the limit $a_0/\ell = -0.11$ is reached, then part of the high-density component is self-bound and the system is expected to collapse.

VI. SUMMARY AND CONCLUSIONS

We formulated a simple and transparent model to describe the structure and stability of degenerate multicomponent Fermi gases trapped in an external potential. In a first step we derived an effective contact interaction (ECI) for all partial waves that reproduces the exact two-body energy spectrum when used in a mean-field model space. Including the s- and p-wave parts of the ECI we constructed the energy density of the inhomogeneous Fermi gas in a mean-field calculation using the Thomas-Fermi approximation. By functional minimization of the energy we obtained a set of coupled polynomial equations for the ground-state density profile of the system. We showed that the combination of s- and p-wave interactions leads to a rich variety of phenomena in trapped degenerate Fermi gases.

In the single-component system the p-wave part is the leading interaction term since s-wave scatterings are prohibited by the Pauli principle. Attractive p-wave interactions cause a mean-field instability of the one-component gas if a certain maximum density is exceeded. We derived explicit stability conditions in terms of the density or particle number and the p-wave scattering length.

The interplay between s- and p-wave interactions leads to several effects in the two-component Fermi gas. We discussed the dependence of the mean-field instability on the s- and p-wave scattering lengths and derived also for this case closed stability conditions. It turns out that attractive s-wave as well as attractive p-wave interactions can cause a mean-field collapse. In addition a repulsive interaction part leads to stabilization, i.e., an increase of the maximum possible density of the Fermi gas.

Interactions with attractive s-wave and repulsive p-wave parts show several special properties. If the p-wave scattering length exceeds about 1/3 of the modulus of the s-wave scattering length the s-wave attraction is fully compensated and no mean-field collapse occurs anymore at high densities. In the transition region towards this absolute stabilization a distinct high-density phase may appear in the center of the trap, which is stabilized by the p-wave repulsion alone.

We conclude that the p-wave interaction may have an important influence on the structure and stability of dilute degenerate Fermi gases. Considering the simultaneous s- and p-wave Feshbach resonances predicted for the ^{40}K system [8] it can be foreseen that large values of p-wave scattering length will be available experimentally. In a two-component ^{40}K gas this Feshbach resonance would allow us to probe nearly the whole stability map shown in Fig. 8 by modifying the magnetic field. Alternatively, tightly confining optical traps [19] generate large values of the ratio of scattering length and oscillator length, a_l/ℓ, such that instabilities occur at much lower particle numbers [$N_{\max} \propto \ell^6$; see Eqs. (70) and (79)].

Concerning the envisioned observation of Cooper pairing in trapped dilute Fermi gases two-component systems with strong attractive s-wave interactions are favored [3,20]. Here the mean-field instability limits the density of the normal Fermi gas. With a suitably chosen repulsive p-wave interaction one could use the effect of absolute stabilization, which we discussed, to allow higher densities of the normal Fermi gas and thus increase the transition temperature to a superfluid state [5].

[1] M. Anderson, J. Ensher, M. Matthews, C. Wieman, and E. Cornell, Science **269**, 198 (1995).

[2] B. DeMarco and D. S. Jin, Science **285**, 1703 (1999).

[3] B. DeMarco, S. B. Papp, and D. S. Jin, Phys. Rev. Lett. **86**, 5409 (2001).

[4] A. Truscott, K. Strecker, W. McAlexander, G. Partridge, and R. Hulet, Science **291**, 2570 (2001).

[5] M. Houbiers, R. Ferwerda, H. T. C. Stoof, W. I. McAlexander, C. A. Sackett, and R. G. Hulet, Phys. Rev. A **56**, 4864 (1997), and references therein.

[6] H. T. C. Stoof and M. Houbiers, in *Proceedings of the International School of Physics—Enrico Fermi*, edited by M. Inguscio, S. Stringari, and C. E. Wieman (IOS Press, Amsterdam, 1999), p. 537.

[7] E. R. I. Abraham, W. I. MacAlexander, J. M. Gerton, R. G. Hulet, R. Cote, and A. Dalgarno, Phys. Rev. A **55**, R3299 (1997).

[8] J. Bohn, Phys. Rev. A **61**, 053409 (2000).

[9] S. Cornish, N. Claussen, J. Roberts, E. Cornell, and C. Wiemann, Phys. Rev. Lett. **85**, 1795 (2000).

[10] R. Roth and H. Feldmeier, J. Phys. B **33**, L787 (2000).

[11] H. Feldmeier, T. Neff, R. Roth, and J. Schnack, Nucl. Phys. A **632**, 61 (1998).

[12] K. Gottfried, *Quantum Mechanics—Volume I: Fundamentals* (Benjamin/Cummings Publishing Inc., Reading, MA, 1966).

[13] *Handbook of Mathematical Functions*, edited by M. Abramowitz and I. A. Stegun (Dover Publications, Inc., New York, 1972).

[14] E. Fermi, Ric. Sci. **7**, 13 (1936).

[15] J. Blatt and V. Weisskopf, *Theoretical Nuclear Physics* (Springer-Verlag, New York, 1979).

[16] K. Huang and C. Yang, Phys. Rev. **105**, 767 (1957).

[17] K. Huang, *Statistical Mechanics* (John Wiley & Sons, New York, 1963).

[18] R. Roth, Ph.D. thesis, Technische Universität Darmstadt, 2000, URL: http://theory.gsi.de/~rroth/phd/.

[19] L. Viverit, S. Giorgini, L. Pitaevskii, and S. Stringari, Phys. Rev. A **63**, 033603 (2001).

[20] K. M. O'Hara, M. E. Gehm, S. R. Granade, S. Bali, and J. E. Thomas, Phys. Rev. Lett. **85**, 2092 (2000).